Supplementary Information

Atmospheric Photo-oxidation of 2-ethoxyethanol: Autoxidation Chemistry of Glycol Ethers

Hongmin Yu [a], Kristian H. Møller [b], Reina S. Buenconsejo [c], John D. Crounse [a], Henrik G. Kjaergaard [b], Paul O. Wennberg [,a,d]*

[a] Division of Geological and Planetary Sciences, California Institute of Technology, 1200 E. California Blvd, Pasadena, CA, 91125

[b] Department of Chemistry, University of Copenhagen, Universitetsparken 5, DK-2100 Copenhagen Ø, Denmark

[c] Division of Chemistry and Chemical Engineering, California Institute of Technology, 1200 E. California Blvd, Pasadena, CA, 91125

[d] Division of Engineering and Applied Science, California Institute of Technology, 1200 E. California Blvd, Pasadena, CA, 91125
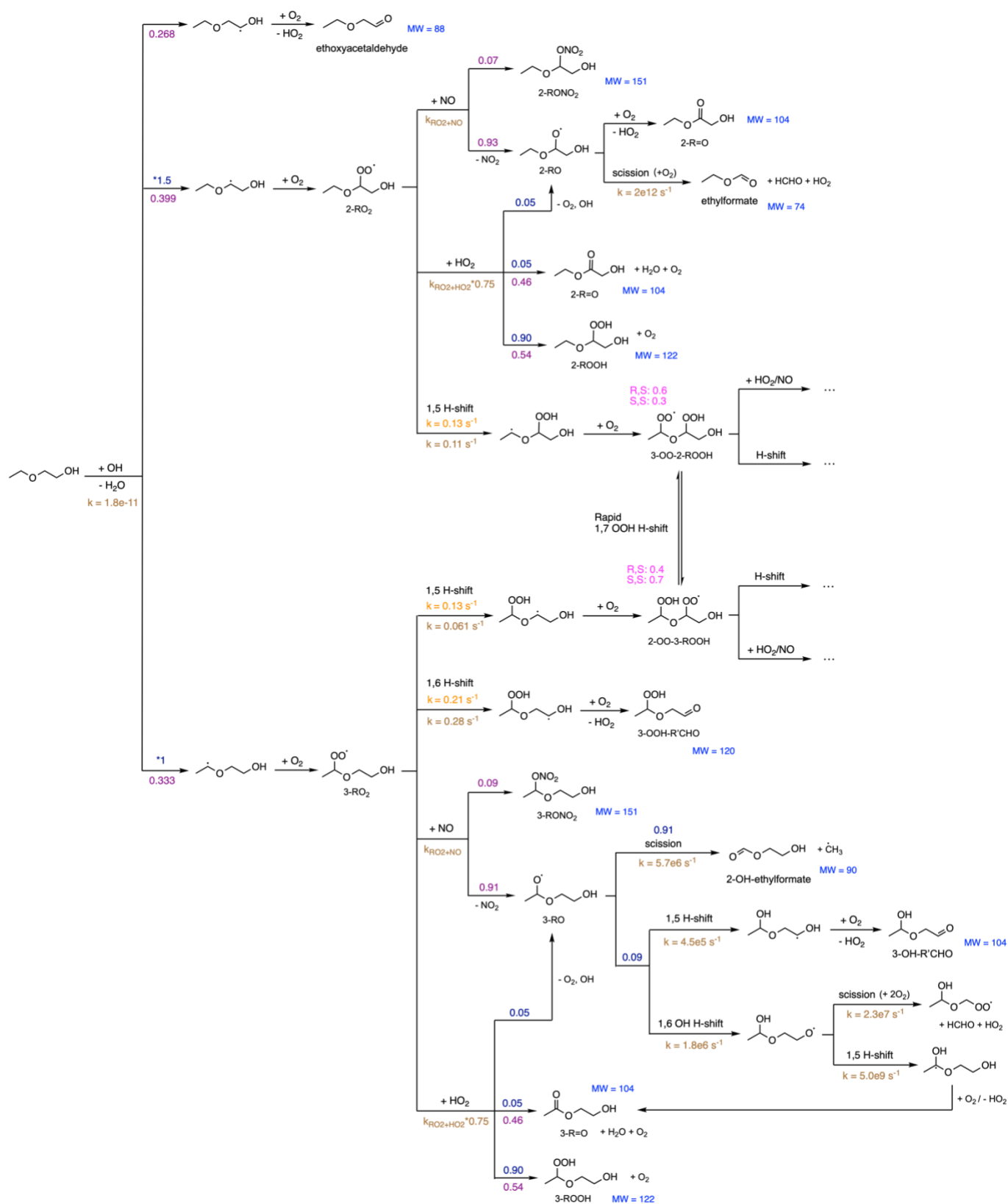
*Correspondence to P.O. Wennberg (wennberg@caltech.edu).
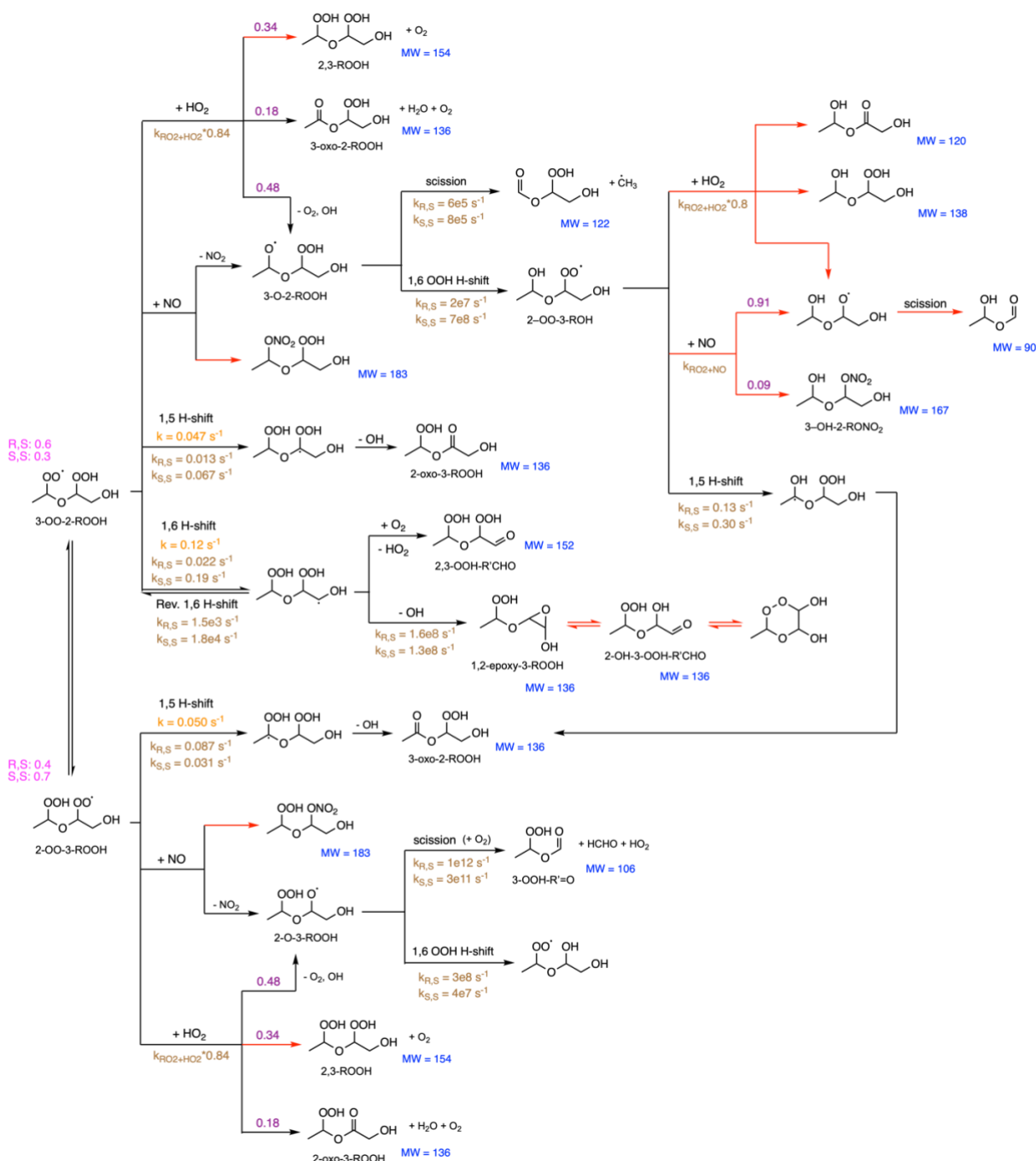
Contents

# 1. Initial steps in the photo-oxidation of 2-ethoxyethanol

Scheme S1. A mechanism of the initial steps in 2-ethoxyethanol (2-EE) photo-oxidation initiated by OH radical (except RO_2 self-reactions). Molecular weights of the products are indicated in blue. The branching ratios and rate coefficients that come from Master Chemical Mechanism (MCM), Jenkin et al.[1], and quantum-chemical calculations are in purple and brown. $k_{RO2+NO} = 2.7 \times 10^{-12} \exp(360/T)$ cm^3 molecule^{-1} s^{-1}. $k_{RO2+HO2} = 2.8 \times 10^{-13} \exp(1300/T)$ cm^3 molecule^{-1} s^{-1}. The branching ratios and rate coefficients determined in this study are in dark blue and orange. The MC-TST H-shift rate coefficients are at 298.15K and the experimental-derived ones are at 294K. The experimental-derived branching fractions of 2-RO_2 and 3-RO_2 formation is normalized by the branching to 3-RO_2, and we are not able to constrain the branching to ethoxyacetaldehyde. The product branching ratios for 2-OO-3-ROOH/3-OO-2-ROOH + HO_2 reactions come from Praske et al.[2] Red arrows indicate reaction pathways yet to be verified.
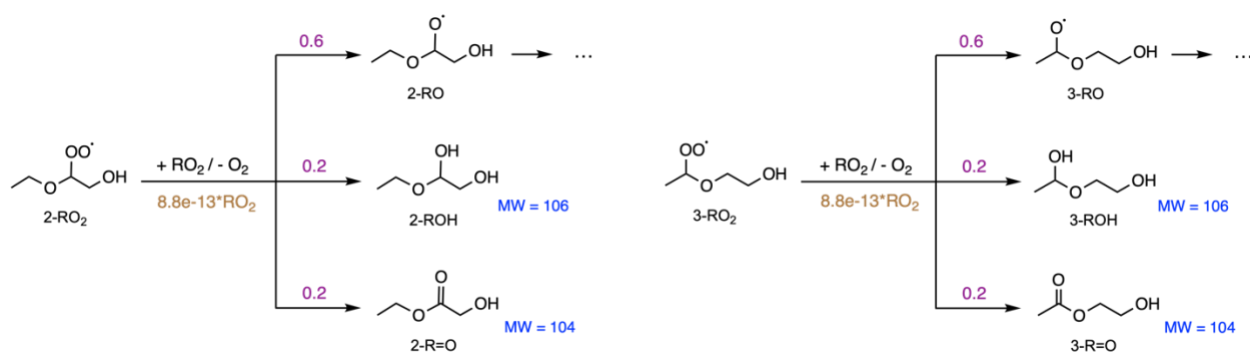
Scheme S2. Mechanism for self-reaction of 2-EE peroxy radicals (RO_2). The branching ratios and rate coefficients come from MCM.

1.1 Box Model Implementation

We implement in the box model a full mechanism of photo-oxidation of 2-EE, i.e., from the starting material (2-EE) to the end-products (CO_2 and H_2O). The full mechanism in .txt is available at: https://doi.org/10.22002/q0x9c-6kr07. The reaction kinetics regarding the formation of first-generation closed-shell products are shown in Scheme S1 and S2. The reaction mechanisms involving multi-generational oxidation products are directly adopted from Master Chemical Mechanism (MCM, mcm.york.ac.uk/home.htt). The following discussion only considers the reactions in Scheme S1, which we can directly examine in this study.

The rate coefficients and branching fractions of initiation reaction 2-EE+OH is initially referred from MCM and Calvert et al.[3], and is later adjusted based on our experimental results. The estimation of the rate coefficients of bimolecular reactions (RO_2+HO_2/NO) relies on the method from Jenkin et al.[1] The branching ratio of RO_2+NO reaction is also adopted from Jenkin et al.[1], while that of RO_2+HO_2 reaction is adopted from the results in this study (Section 2.1), except the 2-OO-3-ROOH/3-OO-2-ROOH + HO_2 reactions whose kinetic information are derived using constraints from the study of methyl vinyl ketone (MVK) by Praske et al.[2] The rate coefficients and branching fractions of unimolecular reactions, including the H-shifts, the reactions of alkoxy radicals, and the equilibrium between 2-OO-3-ROOH and 3-OO-2-ROOH, are initially adopted from quantum-chemical calculations, with some of them adjusted later based on experimental results. The kinetics of photolytic reactions of photo-sensitive compounds, such as hydroperoxides and carbonyls, are detailed in Section S4.1. Other secondary processes, such as vapor wall loss (see Section S4.2), are not explicitly included in the model but are treated separately.

2. Experimental Conditions

All experiments are conducted in a ~0.7 m^3 Teflon chamber. Gas-phase reagents (2-EE, CH_3OH, NO, etc.) were prepared in 500 cm^3 glass bulbs. Desired mixing ratios were achieved through serial dilution using a vacuum/N_2 system, with pressure in the bulbs measured by pressure sensors (MKS 1000 and 10 Torr baraton pressure transducers). Reagents in liquid and solution phase (H_2O_2, ethylene glycol, and other low-volatility organics) were pipetted into three-way glass vials. Their initial mixing ratios in the chamber were determined by weighing the 3-way vial before and after injection. Injection of the reagents was achieved by passing dry air through the bulbs and the vials into the chamber at 20 SLM. The time required to inject the reagents depends on the bag volume and their volatility. For reagents with low volatility, the flow rate of dry air is turned down and their injection time is extended accordingly to facilitate their total evaporation.

After collecting CIMS background signals, we turned the UV lights on to initiate photo-oxidation. The chamber is illuminated ranging from 1 minute to 2 hours depending on the types of UV bulbs used, i.e., the OH radical production rate in the chamber. The oxidation time in the chamber when we use multiple 254nm lights (high OH production rate) was kept short to minimize secondary chemistry. We extended the oxidation time accordingly when fewer bulbs and/or bulbs at lower wavelengths were used so that similar amounts of 2-EE would be oxidized across all experiments. On average, less than 5% of 2-EE was reacted in our experiments (see Table S7).

Upon eluted from the column, the GC effluent is transmitted to the CIMS instrument, either through a Teflon-coated glass flow tube or directly into the ion source, to interact with the CF_3O^- reagent ion to form product ions. We named the former GC operation "normal mode" and the latter "high sensitivity (HS) mode". During normal mode operation, the eluted analytes are mixed with CF_3O^- downstream from the ion source, while in HS mode, the analytes interact with the ions as soon as it forms. Thus, the increase in analyte-reagent ion interaction time in HS mode operation leads to an enhancement in instrument sensitivity of the analytes compared to that in the normal mode. On the other hand, analytes in HS mode are more easily subject to fragmentation due to analyte interactions with the metal walls of the ionizer and the direct electron attachment to analytes. Unless otherwise noted, the experiments listed in the following tables are conducted with normal mode operation.

Table S1. Experimental conditions for 2-EE HO_2 experiments. All concentrations are in ppb. Oxidation time are in minutes. Room temperature (RT) experiments are conducted at $294 \pm 1K$. High temperature experiments at conducted at $309.5 \pm 2K$.

Experiment No.	$[2\text{-}EE]_0$	$[H_2O_2]_0$	$[CH_3OH]_0$	$[Ethylene\ glycol]_0$	Bulb type	Bulb #	Oxidation time	Temperature
1	677	2379	45675	133	254 nm	2	5	RT
2	662	2320	45725	286	254 nm	1	8	RT
							16	
3	559	2133	46539	188	254 nm	7	1.5	RT
							3	
4	675	2297	45771	94	350 nm	8	96	RT
5	631	2488	45771	168	350 nm	8	17	RT
							96	
6	529	2106	46427	197	350 nm	2	68	RT
7	506	2050	48004	222	350 nm	1	136	RT
8	557	1948	47765	211	254 nm	2	5	RT
							12	
9	639	2557	46183	140	254 nm	7	1.5	RT
							2.5	
10	606	2044	46234	206	254 nm	1	8	RT
							16	
11	591	2442	46860	310	254 nm	1	8	HT
12	606	2620	46494	216	254 nm	4	4	HT
13	591	2159	46636	239	350 nm	8	15	HT
							100	
14	626	2389	46697	281	350 nm	1	120	HT
15	602	2284	46254	174	254 nm	8	1	HT

Table S2. Experimental conditions for 2-EE NO experiments. All experiments are conducted at room temperature. Experiment No. 18 are conducted with high sensitivity mode.

Experiment No.	$[2\text{-EE}]_0$	$[H_2O_2]_0$	$[NO]_0$	[Ethylene glycol]$_0$	Bulb type	Bulb #	Oxidation time
16	544	2123	106	347	350 nm	8	16
17	549	2472	592	304	350 nm	8	20
18	667	2073	518	0	350 nm	8	24

Table S3. Experimental conditions for ethyl vinyl ether (EVE) experiments. All experiments are conducted at room temperature. Experiment No. 23 are conducted with high sensitivity mode.

Experiment No.	$[EVE]_0$	$[H_2O_2]_0$	$[CH_3OH]_0$	$[NO]_0$	[Ethylene glycol]$_0$	Bulb type	Bulb #	Oxidation time
19	167	2617	123648	0	261	254 nm	4	5.5
20	181	2267	124266	0	232	350 nm	8	100
21	165	2763	122952	0	172	350 nm	1	120
22	499	1886	0	546	337	350 nm	8	10
23	533	2073	0	522	0	350 nm	8	11

Table S4. Experimental conditions for oxidation of ethyl glycolate (2-R=O) and 2-hydroxyethyl acetate (3-R=O). All experiments are conducted at room temperature.

Experiment No.		$[VOC]_0$	$[H_2O_2]_0$	$[CH_3OH]_0$	Bulb type	Bulb #	Oxidation time
24	**2-R=O**	885	2504	50580	254 nm	8	6
25	**3-R=O**	>822	2342	63240	254 nm	8	8
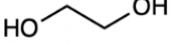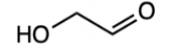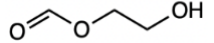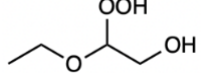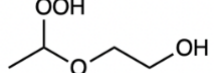
Notes: GC for experiment No.5, 8, and 20 are shown in Figure 1; Experiment No.12 are in Figure S1; Experiment No.5, 20, 24, and 25 are in Figure S2; Experiment No. 17 and 22 are in Figure S3; Experiment No. 18 and 23 are in Figure S4.

3. CIMS Calibration

Quantification of oxidation products is achieved by measuring the product ions clustered with CF_3O^- reagent ion (m/z 85), with a detection limit of ~10 ppt and with a 1 sec integration period. CF_3O^- readily clusters with H_2O and H_2O_2, producing high signals observed at m/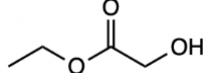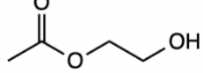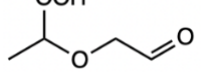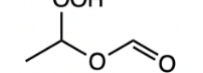z 103 and 119. Thus, to compensate for the variation in the total ion signal, the analyte signals were normalized to the sum of the isotope of the reagent ion, $^{13}CF_3O^-$ (m/z 86), and its clusters with H_2O and H_2O_2 (m/z 104 and m/z 120). We use the isotopologs of these reagent ion clusters at m/z + 1 to normalize the analyte signals in order to remain in a linear counting regime due to the high numbers of these reagent ions. Therefore, the sensitivities listed in Table S5 below are normalized by the sum of m/z 86 + m/z 104 + m/z 120.

Since we lack authentic standards for most of the species discussed in this study, direct calibration is not possible. The CIMS sensitivities of 2-EE oxidation products are thereby estimated through the calculation of the CF_3O^--molecule collision rate coefficients from the parameterization of Su et al.[4] using calculated dipole moments and polarizabilities of the molecules. The dipole moments and polarizabilities of closed-shell products are calculated at B3LYP/cc-pVTZ level. The dipole moment is calculated based on the weighted average of the located conformers due to the dependence of the dipole moment on structural conformation, while the polarizability does not exhibit large conformational dependence and is based on the lowest energy conformer.[5] The sensitivities of the oxidation products are calibrated based on the ion-molecule collision rate and measured sensitivity for ethylene glycol.[6]

Table S5. Calculated dipole moments (α), polarizabilities (μ_D), CF_3O^--molecule collision rate coefficients (k_c), and CIMS sensitivities for molecules of interests in our system. [a] Normalized relative to that of ethylene glycol. [b] Measured sensitivity data and uncertainties for ethylene glycol and glycoaldehyde come from Murphy et al.[6]

Molecule	m/z	α (Å^3)	μ_D (D)	k_c (10^{-9} cm^3 molecule^{-1} s^{-1})	Relative k_c [a]	Sensitivity (10^{-4} cts/pptv)
Ethylene glycol	147	2.08	5.11	1.90	1	2.50 ($\pm$ 0.20)[b]
Glycolaldehyde	145	2.33	4.64	2.06	1.08	2.71 ($\pm$ 0.22)[b]
2-OH-ethylformate	175	3.77	7.06	2.80	1.47	3.69 ($\pm$ 0.30)
2-ROOH	207	2.72	10.0	2.14	1.13	2.82 ($\pm$ 0.23)
3-ROOH	207	2.97	10.1	2.29	1.20	3.01 ($\pm$ 0.24)
2-R=O	189	3.15	8.77	2.42	1.27	3.19 ($\pm$ 0.26)
3-R=O	189	2.76	8.70	2.20	1.16	2.89 ($\pm$ 0.23)
3-OOH-R'CHO	205	4.14	9.55	2.92	1.54	3.84 ($\pm$ 0.31)
3-OOH-R'=O	191	3.01	7.76	2.30	1.21	3.02 ($\pm$ 0.24)

Molecule	m/z	α (Å³)	μ_D (D)	k_c (10^{-9} cm³ molecule⁻¹ s⁻¹)	Relative k_c	Sensitivity (10^{-4} cts/pptv)
2-oxo-3-ROOH	221	3.08	10.1	2.29	1.21	3.02 (± 0.24)
3-oxo-2-ROOH	221	3.48	10.1	2.51	1.32	3.31 (± 0.27)
(R,R)-2-OH-3-OOH-R'CHO	221	2.79	10.2	2.14	1.12	2.81 (± 0.23)
(R,S)-2-OH-3-OOH-R'CHO	221	2.78	10.2	2.14	1.12	2.81 (± 0.23)
(R, R, R)-epoxide	221	2.93	10.0	2.21	1.16	2.91 (± 0.23)
(S, R, R)-epoxide	221	2.91	9.92	2.20	1.16	2.89 (± 0.23)
2-RONO₂	236	2.69	11.7	2.09	1.10	2.75 (± 0.22)
3-RONO₂	236	2.795	11.6	2.15	1.13	2.82 (± 0.23)

4. Secondary Losses

To evaluate the production rate of 2-EE oxidation products from the measured yields, we need to account for their secondary losses. The loss processes we considered in this study include: photolysis, vapor wall loss, and loss during GC transmission.
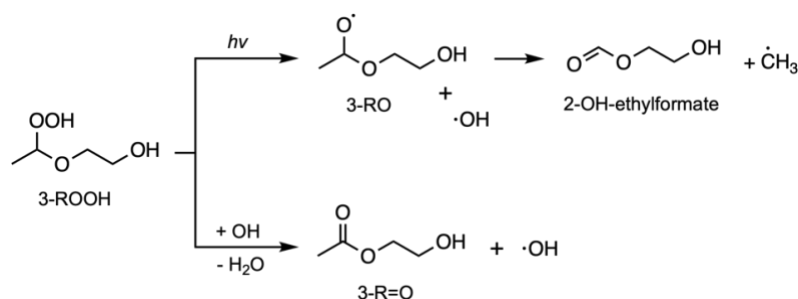
4.1 Photolysis

The major compound classes we considered to potentially undergo photolysis during irradiation are the hydroperoxides and carbonyls (ketones and aldehydes). We estimate the photolysis rates of those compounds as follows (similar procedure also described in Murphy et al.[6]):

We first synthesized the oxidation products at relatively higher yields in the chamber (by oxidizing under 254nm UV lights for an extended period). Then we evacuated the chamber through a coil made from Teflon tubes while submerging the coil in an ethanol/liquid nitrogen bath maintained at approximately $-30°C$. In this way, we expect that the low-volatility products, most of which consist of hydroperoxide and carbonyl moieties, would be trapped in the coil and 2-EE, H_2O_2, and other high-volatility products to be pumped away. After that, we cleaned out the chamber by flushing it thoroughly with clean air, and returned the contents trapped in the Teflon coil back to the chamber by slowly passing dry air through the coil. Finally, we injected ~90 ppm CH_3OH into the chamber as a ·OH scrubber to minimize the influence from secondary chemistry other than photolysis. We then turned on the UV lights and examine the evolution of relevant compounds.

From the photolysis experiment, we observe a decrease in [3-ROOH], which approximately equals to the sum of the increase in [2-OH-ethylformate] and [3-R=O] (Table S6). 2-OH-ethylformate is likely a product from photolysis of 3-ROOH, while 3-R=O is formed by oxidation of 3-ROOH by OH radical (Scheme S3). From the production of 2-OH-ethylformate, we manage to estimate the photolysis frequency for the ROOH's (Table S5). We expect that the true photolysis rate coefficients of the peroxides is close to that of H_2O_2, which is $1.7×10^{-6}$ s^{-1} under eight 350nm bulbs and $2.7×10^{-4}$ s^{-1} under eight 254nm bulbs in our chamber. Our estimate is within reasonable agreement of the expected values. Still, under conditions when we lack necessary data to evaluate the photolytic loss, we assume that the photolysis rate coefficients of all other ROOH's is equal to that of H_2O_2.

We were unable to identify any trends in the concentrations of aldehydes or ketones that could be useful for quantifying their photolytic loss. Therefore, for photolysis frequencies of those compounds, we adopt measurements of similar compounds from the literature.[7–10] For compounds with multiple types of moieties, we account for their photolysis frequencies from the sum of the photolysis rate coefficients of relevant compound classes.

We list the estimates for the photolysis rate coefficients of the hydroperoxides and carbonyls in Table S5. The photolysis frequencies listed in the table are evaluated under our chamber conditions with eight 254nm bulbs and eight 350nm bulbs. Since the light intensities of the bulbs increase as they warm up over time, the photolysis frequencies for different experiments with varied light intensities and oxidation time are evaluated based on the mean irradiance in the chamber during oxidation, using time-dependent measurements of cosine-corrected irradiance of the bulbs (Ocean Optics spectrometer integrated between 224 and 284nm). The H_2O_2 photolysis frequencies at 254nm in Table S5 were calculated based on the mean irradiance of the bulbs over the 90 sec time period of our experiments, and the photolysis frequencies of other compounds are scaled accordingly. For the photolysis frequencies of the compounds at 350nm with lower light intensities, since we lack time-dependent data of bulb irradiation, they are directly scaled from the values evaluated with eight light bulbs. As a result, based on our estimations of the photolysis frequencies, we calculate that around 2-5% of those potentially photo-sensitive compounds were lost during the experiments due to photolysis.

Scheme S3. Potential secondary chemistry pathways of 3-ROOH

Table S6. Estimated photolysis frequencies (in s^{-1}) of relevant compound classes in the system. [a] H_2O_2 photolysis frequency in our chamber at 254nm is calculated by Murphy et al.[6] by measuring OH production via the decay of 2,3-butanediol, and scaled to fit our experiment conditions. The photolysis frequency at 350nm is calculated using similar method via the decay of ethylene glycol. [b] Photolysis frequency of ROOH at 350nm is evaluated from the results of photolysis experiments. [c] Photolysis frequency of aldehydes at 254nm is adopted from measurements by Murphy et al.[6] on the photolysis of glycoaldehyde. The rate coefficient at 350nm is inferred from UV absorption spectrum of similar aldehydes with long carbon chain.[7,10] [d] Photolysis frequencies of ketones are inferred from UV absorption spectrum of similar compounds[8] based on literature values of their photolysis frequencies at different wavelengths.[9]

Wavelength	H_2O_2 [a]	Hydroperoxides [b] (ROOH)	Aldehydes [c] (R'CHO & R'=O)	Ketones [d] (R=O)
254 nm	$2.7 (\pm 0.4) \times 10^{-4}$	$2.7 (\pm 0.4) \times 10^{-4}$	$1.7 (\pm 0.1) \times 10^{-4}$	$7.3 (\pm 0.8) \times 10^{-5}$
350 nm	$1.7 (\pm 0.2) \times 10^{-6}$	$1.4 (\pm 0.2) \times 10^{-5}$	$1.7 (\pm 0.1) \times 10^{-6}$	$6.1 (\pm 0.7) \times 10^{-6}$

Table S7. Results from the photolysis experiment. Change in the abundance of selected oxidation products before and after photolysis. All concentrations are in ppb. The experiment is conducted using 8 350nm bulbs and photolyzed for 60 min.

	[2-OH-ethylformate]	[2-ROOH]	[3-ROOH]	[3-R=O]
initial	0.093	0.51	0.28	0.36
final	0.106	0.32	0.17	0.45
Δ	0.013	− 0.19	− 0.11	0.09

4.2 Vapor Wall Loss

Vapor wall loss is the partition of organic vapor products onto the chamber walls. We attempt to estimate the wall loss of 2-EE oxidation products by measuring the dark decay of those compounds after oxidation. Fitting the decay of the low-volatility compounds gives a wall loss rate for the ROOH's to be $2.5(\pm 0.4)\times10^{-6}$ s^{-1}, and the ketohydroperoxides (2-oxo-3-ROOH and 3-oxo-2-ROOH) to be $6.1(\pm 0.9)\times10^{-6}$ s^{-1}, which would on average lead to around 2% loss for the compounds over 1 hour. Those values are smaller than our expectation, especially for the ketohydroperoxides, as these compounds are both highly oxygenated and functionalized. They are expect to have low volatility and would readily partition into the condensed phase.[11]

One reason for the potential underestimation is likely that the low-volatility vapor equilibrates relatively fast between the gas-phase and the wall-phase. For low vapor pressure species, vapor-wall equilibrium can be established in relatively short timescale (~10 min in bag).[12] Smaller the vapor-wall equilibrium timescale of the compounds, earlier the wall loss process start to take effect on their detectable gas phase concentration.[12–14] The compound likely already start to approach gas-wall equilibrium during the oxidation period, which would result in a smaller decay observed after the oxidation. Thus, the detected long-timescale wall-loss likely only encompasses a portion of vapor-wall partitioning. Other dark loss processes, e.g., reactive uptake by the walls, diffusion of species into the Teflon, or dilution due to potential leaks, may also account for the detected decay. Still, we expect that the underestimation in vapor-wall losses of the compounds will not greatly affect our results. Most analysis in this study is based on the ratios between concentrations of relevant hydroperoxides (e.g. [2-ROOH]/[3-ROOH] in Section 2.3, and [3-oxo-2-ROOH]/[2-oxo-3-ROOH] in Section 2.5), so as long as the wall loss of those compounds are similar (see Table S8 for a list of vapor pressure estimated by EVAPORATION[15]), it should have small impact on our results.

However, the potential underestimation in wall partitioning for certain compounds can lead to biases in our estimations of some parameters. For example, 3-ROOH may have larger vapor-wall loss than our estimation here, which would lead to underestimation in its branching fraction in Section 2.1, underestimation in [3-ROOH]/[3-OOH-R'CHO] and overestimation in

$k_{1,6\ H-shift,3-RO_2}$ in Section 2.2, and overestimation in [2-ROOH]/[3-ROOH] and biases in the 1,5 H-shift rate coefficients in Section 2.3. Moreover, the ketohydroperoxides also likely have higher magnitude of wall loss, which may lead to biases in [3-oxo-2-ROOH]/[2-oxo-3-ROOH] in Section 2.5.

Table S8. Vapor pressure (in atm) of major oxidation products in 2-EE system estimated by EVAPORATION method[15] at 294K. (https://tropo.aeronomie.be/index.php/models/evaporation)

	2-ROOH	**3-ROOH**	**2-R=O**	**3-R=O**
Vapor Pressure (in atm)	2.8×10^{-6}	2.0×10^{-6}	6.3×10^{-4}	5.3×10^{-4}
	3-OOH-R'CHO	**3-OOH-R'=O**	**2-oxo-3-ROOH**	**3-oxo-2-ROOH**
Vapor Pressure (in atm)	1.9×10^{-4}	6.8×10^{-4}	4.0×10^{-7}	5.4×10^{-7}

4.3 GC Transmission

A certain portion of the oxidation products are lost by decomposition and/or reaction with the column surface as they are travelling through the column. The GC transmission rates of the products are evaluated by comparing their detected concentrations from direct sampling mode and GC mode. Losses are often greater for compounds eluting later at higher temperature. On average, the products elute before ~10 min (2-OH-ethylformate, 3-R=O, and 3-OOH-R'=O) have GC transmission rates of ~90%. The products with hydroperoxy group (3-OOH-R'CHO, 2-ROOH, and 3-ROOH) have transmission rates of 60-70%. The ketohydroperoxides (2-oxo-3-ROOH and 3-oxo-2-ROOH), due to their low volatility and multifunctionality as mentioned in Section 2.5, have low GC transmission rates of 25-30%.

5. Table of Results

Table S9. Experimental results with all data corrected. All concentrations are in ppb. HO_2 concentrations are determined by the box model.

Experiment No.	[HO₂]	Δ[2-EE]	[2-OH-ethylformate]	[3-R=O]	[3-ROOH]	[2-ROOH]
1	1.42	20.2	0.31	0.24	4.88	9.51
2	1.04	10.0	0.15	0.12	2.49	5.08
		19.0	0.29	0.24	4.73	9.46
3	2.27	8.95	0.12	0.13	2.89	4.70
		18.5	0.25	0.28	5.59	9.41
4	0.19	15.4	0.09	0.09	0.76	2.19
5	0.20	1.84		0.01	0.11	0.34
		11.7	0.05	0.07	0.50	1.59
6	0.10	1.50	0.02	0.005	0.05	0.18
7	0.07	1.62		0.002	0.05	0.18
8	1.33	9.39	0.13	0.15	3.25	6.38
		25.0	0.44	0.50	6.15	12.40
9	2.42	10.1	0.12	0.13	2.43	4.04
		16.3	0.23	0.23	4.05	7.21
10	0.99	6.15	0.04	0.05	1.11	2.32
		12.8	0.10	0.12	1.83	4.26
11	1.42	9.11	0.05	0.05	1.05	2.71
12	2.85	18.2	0.12	0.16	3.77	8.73
13	0.23	1.62	0.01	0.002	0.03	0.10
		11.4	0.05	0.04	0.19	0.62
14	0.08	2.91	0.01	0.01	0.02	0.06
15	3.73	8.45	0.06	0.08	1.69	3.61

Experiment No.	[HO₂]	Δ[2-EE]	[3-OOH-R'CHO]	[3-OOH-R'=O]	[3-oxo-2-ROOH]/[2-oxo-3-ROOH]
1	1.42	20.2	1.63	0.53	
2	1.04	10.0	1.29	0.39	
		19.0	2.46	0.88	
3	2.27	8.95	0.69	0.20	
		18.5	1.30	0.43	
4	0.19	15.4	1.58	0.84	
5	0.20	1.84	0.21	0.09	
		11.7	1.19	0.63	1.54
6	0.10	1.50	0.17	0.07	1.45
7	0.07	1.62	0.20	0.07	1.29
8	1.33	9.39	1.26	0.39	1.67
		25.0	2.55	1.00	1.60
9	2.42	10.1	0.55	0.17	
		16.3	0.94	0.32	1.49
10	0.99	6.15	0.67	0.21	
		12.8	1.11	0.41	1.75
11	1.42	9.11	1.59	0.75	1.60
12	2.85	18.2	2.80	1.16	1.56
13	0.23	1.62	0.17	0.08	1.47
		11.4	1.00	0.57	1.48
14	0.08	2.91	0.14	0.07	1.35
15	3.73	8.45	3.61	0.95	1.46

6. Estimation of Uncertainties

6.1 HO₂ Concentrations

The rates for the dominant production and loss of HO_x species in our experiments are given by:

$$P(OH) = 2 J_{H_2O_2}[H_2O_2] \qquad (S1)$$

$$L(OH) = (k_{OH+H_2O_2}[H_2O_2] + k_{OH+CH_3OH}[CH_3OH] + k_{OH+ 2-EE}[2 - EE])[OH] \qquad (S2)$$

$$P(HO_2) = (k_{OH+H_2O_2}[H_2O_2] + k_{OH+CH_3OH}[CH_3OH] + \alpha \cdot k_{OH+ 2-EE}[2 - EE])[OH] \qquad (S3)$$

$$L(HO_2) = 2k_{HO_2+HO_2}[HO_2]^2 + k_{RO_2+HO_2}[RO_2][HO_2] \qquad (S4)$$

Following their formation via the photolysis of H_2O_2, OH radicals are consumed through reactions with H_2O_2 (k = 1.8×10^{-12} cm³ molecules⁻¹ s⁻¹ based on Vakhtin et al.[16]), CH_3OH (k = 8.8×10^{-13} cm³ molecules⁻¹ s⁻¹ at 294K based on MCM), and 2-EE (k = 1.8×10^{-11} cm³ molecules⁻¹ s⁻¹ based on MCM and literature values[3,17–20]). The same reactions are also sources for HO_2 in the system. α in Equation S3 indicates the branching ratio for HO_2 production through reaction of 2-EE and OH. The major loss of HO_2 is its self-reaction and its reaction with RO_2. In our experiments, the concentration of CH_3OH (~46 ppm, 1.1×10^{15} molecules/cm³) is much higher than 2-EE (~600 ppb, 1.5×10^{13} molecules/cm³) (see Table S1 for list of experimental conditions), and so that approximately 80% of OH radical reacts with H_2O_2 and CH_3OH, and less than 20% reacts with 2-EE. As a result, Equations S2-S4 can be simplified as:

$$L(OH) \cong (k_{OH+H_2O_2}[H_2O_2] + k_{OH+CH_3OH}[CH_3OH])[OH] \qquad (S5)$$

$$P(HO_2) \cong (k_{OH+H_2O_2}[H_2O_2] + k_{OH+CH_3OH}[CH_3OH])[OH] \qquad (S6)$$

$$L(HO_2) \cong 2k_{HO_2+HO_2}[HO_2]^2 \qquad (S7)$$

Assuming steady state for OH and HO₂ equalizes the equations above and gives:

$$2 J_{H_2O_2}[H_2O_2] \cong 2k_{HO_2+HO_2}[HO_2]^2 \qquad (S8)$$

$$[HO_2] \cong \sqrt{\frac{J_{H_2O_2}[H_2O_2]}{k_{HO_2+HO_2}}} \qquad (S9)$$

Therefore, [HO₂] is approximately proportional to the square root of the photolysis rate coefficient of H_2O_2, which can be varied by changing the number and wavelengths of UV lamps in our chamber enclosure.

Based on Equation S9, the HO$_2$ concentrations in our system are constrained by the photolysis frequencies of H$_2$O$_2$, H$_2$O$_2$ concentrations, and the rate coefficient of the self-reaction of HO$_2$. We determine the uncertainties in the photolysis frequencies of H$_2$O$_2$ by the uncertainty in the fitted slopes used to evaluate these photolysis rate coefficients (Table S5). The major uncertainties in [H$_2$O$_2$] arise from our sample preparation procedure and instruments, and we estimate that it induces about systematic $\pm$ 20% error in the determined [H$_2$O$_2$]. We evaluate the uncertainty in $k_{HO_2+HO_2}$ to be $\pm$ 21% at lab temperature, and $\pm$ 23% at high temperature based on the method in JPL documentation.[21] Thus, the resulting uncertainty in the estimated [HO$_2$] in our experiments equals ~17%.

6.2 Product Concentrations and Ratios of Product Yields

The major source of uncertainties in the measured concentrations of oxidation products, as well as the ratio between the concentrations, lies in the instrument sensitivity of the product. The uncertainty in the measured sensitivities is calculated as the standard deviation of replicate measurements.[6] Part of the uncertainty in the calculated sensitivities are determined by propagating the error in the measured ethylene glycol sensitivity (Table S8), which is around $\pm$ 8%. Since this component of error (calculated sensitivities) is correlated, it cannot be used simply to propagate the error in the ratios of product yields. Another source of uncertainty in the sensitivities comes from the error in calculated ion-molecule rate coefficients, which can be determined by propagating the error in the calculated polarizabilities and dipole moments.[5] The resulted ~20% error is not correlated by common measurements and thus can be used to infer the uncertainties in the ratios between the yields of different products. Therefore, we evaluate the uncertainty in the concentrations of detected products to be ~21%, while the uncertainty in the ratios of product concentrations to be ~25%.

6.3 Amount of Oxidized 2-ethoxyethanol and Normalized Product Yields

In order to calculate the amount of 2-EE consumed (Δ[2-EE]) during the experiments, we add ethylene glycol (EG) into our chamber and measure its oxidation product glycoaldehyde (GA). We start with the rate equations for the loss of 2-EE and EG and the production of GA:

$$\frac{d[2-EE]}{dt} = -k_{2-EE+OH}[2-EE][OH] \qquad (S10)$$

$$\frac{d[EG]}{dt} = -k_{EG+OH}[EG][OH] = -\frac{d[GA]}{dt} \qquad (S11)$$

By assuming that the amount of 2-EE and EG oxidized is much smaller than the initial concentrations of the two compounds, we can simplify the equations as:

$$\frac{\Delta[2-EE]}{\Delta t} \cong -k_{2-EE+OH}[2-EE]_i[OH] \qquad (S12)$$

$$\frac{\Delta[EG]}{\Delta t} = -\frac{\Delta[GA]}{\Delta t} \cong -k_{EG+OH}[EG]_i[OH] \quad (S13)$$

Rearranging and combining the Equations S12 and S13 gives us the expression to estimate Δ[2-EE]:

$$\Delta[2-EE] \cong [2-EE]_i \cdot \frac{\Delta[GA]}{[EG]_i} \cdot \frac{k_{2-EE+OH}}{k_{EG+OH}} \quad (S14)$$

Thus, Δ[2-EE] is constrained by the following quantities: the ratio between the concentrations of EG and GA, the initial concentration of 2-EE, and the rate coefficients of 2-EE and EG oxidation reaction by OH. We have the uncertainties in the ratios between the concentrations of detected species from the previous section (25%). The major source of uncertainty in [2-EE] arises from our sample preparation procedure (Section S2), and the error is likely to be small. We adopt the error in the rate coefficients from their literature values,[3,17–19,22,23] which is ~25% for $k_{2-EE+OH}$ and ~18% for k_{EG+OH}. As a result, we are able to determine the uncertainty in Δ[2-EE] to be ± 40%, and the normalized yield of oxidation products from our measurements, which equals to the concentration of the product divided by Δ[2-EE], to be ± 45%.

Table S10. Sources of uncertainties for reaction parameters determined in this study. [a] Values at room temperature (294K). [b] Values at high temperature (309.5K). [c] Uncertainty in $k_{RO_2+HO_2}$ of 2-EE RO_2 are derived from that of $C_2H_5O_2^{\bullet}$.[21]

Quantity	Constraints	Sources of Uncertainty	Value
$\alpha_{4a}\ (k_{4a}/k_4)$	$\dfrac{[2-OH-ethylformate]}{[3-ROOH]}$	Fit Fig. 5a (13%), $\dfrac{[2-OH-ethylformate]}{[3-ROOH]}$ (25%)	0.896 ± 0.026^a, 0.936 ± 0.016^b
$\alpha_{4b}\ (k_{4b}/k_4)$	$\dfrac{[3-R=O]}{[3-ROOH]}$	Fit Fig. 5b (10%), $\dfrac{[3-R=O]}{[3-ROOH]}$ (25%)	0.048 ± 0.013^a, 0.035 ± 0.009^b
$\alpha_{4c}\ ((k_{4c.1}+k_{4c.2})/k_4)$			$0.056 \pm 0.016^{\,a}$, 0.029 ± 0.009^b
$(k_{4c.1}+k_{4c.2})/k_{4c.3}$	$\dfrac{[3-R=O]+[3-OH-R'CHO]}{[2-OH-ethylformate]}$	Fit Fig. S1 (3%), $\dfrac{[3-R=O]+[3-OH-R'CHO]}{[2-OH-ethylformate]}$ (25%)	0.0954 ± 0.024
Slope Fig. 6 $\left(\dfrac{\alpha_{4a}k_{RO_2+HO_2}}{k_{1,6\ H-shift,3-RO2}}\right)$	$\dfrac{[3-ROOH]}{[3-OOH-R'CHO][HO_2]}$	Fit Fig. 6 (2%), $\dfrac{[3-ROOH]}{[3-OOH-R'CHO]}$ (25%), $[HO_2]$ (17%)	$(7.33 \pm 2.21) \times 10^{-11\ a}$ $(1.95 \pm 0.59) \times 10^{-11\ b}$
$k_{1,6\ H-shift,3-RO_2}$	$\dfrac{k_{RO_2+HO_2}}{(slope\ fig.6)}$	$k_{RO_2+HO_2}$ (52%)[c], slope Fig. 6 (30%)	$0.21 \pm 0.13^{\,a}$, $0.67 \pm 0.42^{\,b}$
$\dfrac{\alpha_{2-RO_2}}{\alpha_{3-RO_2}}$		$\dfrac{[2-ROOH]}{[3-ROOH]}$ (25%)	1.5 ± 0.4
$\alpha_{3-RO_2}+\alpha_{2-RO_2}$	Normalized [2-ROOH] + [3-ROOH] (45%), α_{4a} (29%)		$0.8+0.2/-0.4$
$k_{1,5\ H-shift,2-RO_2}$	Normalized [2-ROOH] (45%), α_{4a} (29%), $k_{RO_2+HO_2}[HO_2]$ (56%)		0.13 ± 0.10^a, 0.54 ± 0.42^b
$k_{1,5\ H-shift,3-RO_2}$	Normalized [3-ROOH] (45%), α_{4a} (29%), $k_{RO_2+HO_2}[HO_2]$ (56%)		0.13 ± 0.10^a, 0.59 ± 0.46^b
H-shift rate coefficients of 2-OO-3-ROOH and 3-OO-2-ROOH	H-shift rate coefficients of 2- and 3-RO_2 (77%), $k_{RO_2+HO_2}[HO_2]$ (56%), $\dfrac{[2-OO-3-ROOH]_{eq}}{[3-OO-2-ROOH]_{eq}}$ (27%), Normalized [3-OOH-R'=O] (56%), $\alpha_{3-RO_2}+\alpha_{2-RO_2}$ (53%)		See Table 3, Monte Carlo method is applied to derive the difference between plus and minus error.

7. Additional Results

7.1 GC peak assignments

To assign the m/z 191 signal to 3-OOH-R'=O, we use deuterium exchange experiments to eliminate from consideration the exact mass isomers, i.e., the diols 2-ROH and 3-ROH shown in Scheme S2, which would be produced in reactions of 2-RO$_2$ and 3-RO$_2$ with themselves or with each other (through RO$_2$+RO$_2$ chemistry). 3-OOH-R'=O has only one readily exchangeable hydrogen, while the diols have two. With addition of D$_2$O to the GC effluent, analytes with exchangeable H's will undergo H/D exchange with the hydrogen replaced by deuterium, and signals of compounds with n exchangeable H's will shift up by n m/z. Deuteration of GC effluent is achieved by passing dry N$_2$ through D$_2$O (99.9%, Cambridge Isotope Laboratories, Inc.) into the flow tube (through which the GC effluent is transmitted to the CIMS) during GC sampling. Figure S1 shows the gas chromatograms from a HO$_2$ experiment after deuteration. Consistent with our assignments, the signal of ROOH's and oxo-ROOH's shift up by 2 m/z, and the signal of 2-OH-ethylformate, 3-R=O, and 3-OOH-R'CHO shift up by 1 m/z. The peak at m/z 191 also shifts up by 1 m/z, and no signal at m/z 193 beyond the contribution of the ^{13}C isotope is observed.
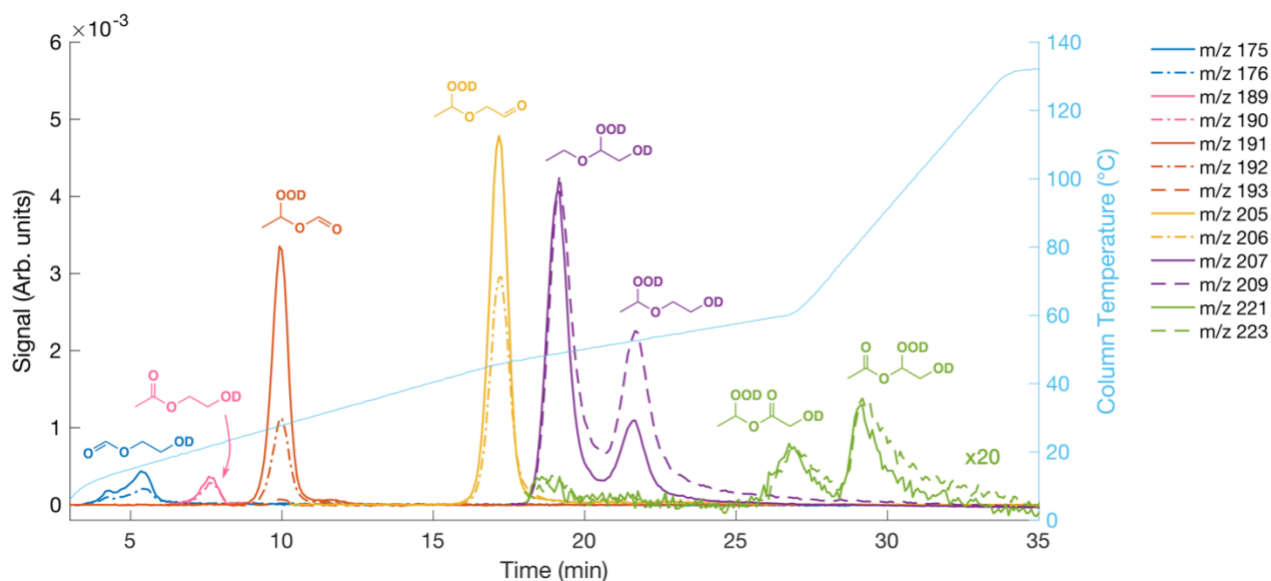

Figure S1. Gas chromatograms of deuterated oxidation products from a 2-EE HO$_2$ experiment. Signals for original product m/z are in solid line. m/z + 1 signals are in dash-dotted line, and m/z + 2 signals are in dashed line. The signals at m/z 221 and m/z 223 are scaled up by a factor of 20.

The assignment of GC peaks at m/z 189 and m/z 221 is facilitated by oxidizing 2-R=O and 3-R=O standards, ethyl glycolate (Sigma Aldrich, 98%) and 2-hydroxyethyl acetate (TCI, >60%), under high [HO$_2$] condition. The resulted gas chromatograms are shown in Figure S2(c). Comparing with the peaks at the same m/z from a 2-EE (Figure S2(a)) and an EVE experiment (Figure S2(b)), we are able to identify the 2-R=O and 3-R=O peaks (at m/z 189), as well as the two m/z 221 peaks eluting at higher temperature.
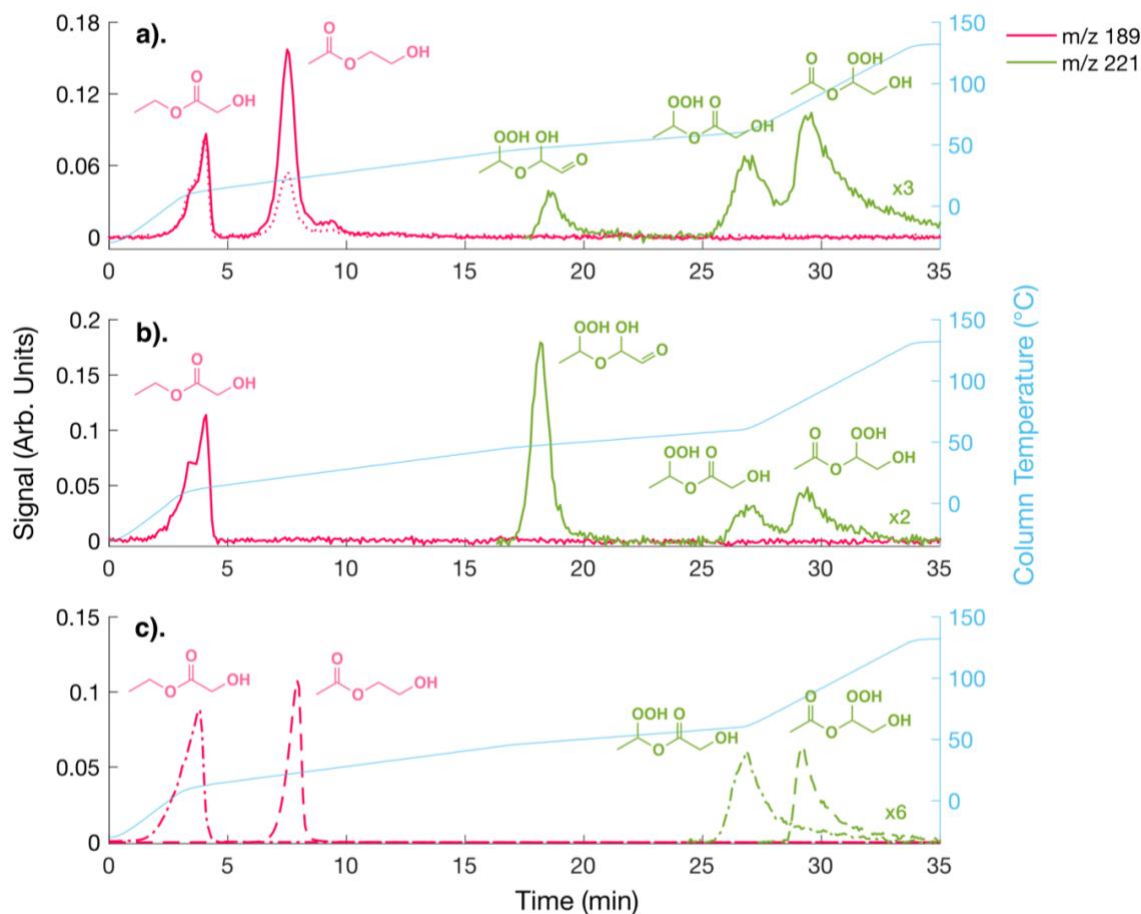
Figure S2. Gas chromatograms of products at m/z 189 (2-R=O and 3-R=O) and m/z 221 (2-OH-3-OOH-R'CHO, 2-oxo-3-ROOH, and 3-oxo-2-ROOH) from **a)**. a 2-EE HO$_2$ experiment; **b)**. an EVE HO$_2$ experiment, **c)**. oxidation of ethyl glycolate (2-R=O, in dash-dotted line) and 2-hydroxyethyl acetate (3-R=O, in dashed line). The m/z 221 signals in the figure are all scaled up by certain factors denoted in the figure. The pink dotted line in **(a)** indicates the m/z 189 signals from the oxidation run prior to the run of GC signals in pink solid line.

From Figure S2(a) and (b), we notice that the peak assigned to 2-R=O (the first peak) obtain an irregular shape. We further notice that the GC signal of 2-R=O does not increase with illumination, unlike other oxidation products in the system. As shown in the dotted and solid pink line in Figure S2(a), which represents m/z 189 signals from two consecutive oxidation runs, there is minimal difference in 2-R=O signals between the two runs. Such phenonmenon hampers our efforts to measure 2-R=O quantitatively. One explanation is that the signal at m/z 189 may arise from some unknown impurities (or other unrecognized products) that elutes at similar temperature as 2-R=O, which may account for the irregular peak shape in Figure S2(a) and (b). Another possibility is that the unusual peak shape indicates peak fronting in chromatography. The compound is likely not trapped efficiently in the column. The observed signal may only correspond to the amount that is adsorbed to the column phase during each GC run, which explains the unchanged signal across runs.

7.2 Results from Experiments with NO

Shown in Figure S3 are the gas chromatograms of products formed in oxidation experiments of 2-EE and EVE at high [NO] (~500 ppb; ~1.2×10^{13} molecules/cm^3). These experiments enable us to identify 2-OH-ethylformate (m/z 175), 3-R=O and 3-OH-R'CHO (m/z 189, 3-OH-R'CHO likely corresponds to the unresolved shoulder at slightly lower temperature of the major peak), which are major products from reactions of alkoxy radical 3-RO, and two hydroxynitrates 2-RONO$_2$ and 3-RONO$_2$ (m/z 236). Oxidation of EVE differentiates the two nitrate peaks from 2-EE experiments, with 2-RONO$_2$ eluting at lower temperature and 3-RONO$_2$ at higher temperature. We also observe products from autoxidation pathways in these experiments, such as 3-OOH-R'CHO (m/z 205) and 3-OOH-R'=O (m/z 191). Given the short bimolecular lifetime (~0.01s), the product yields of those compounds are low.
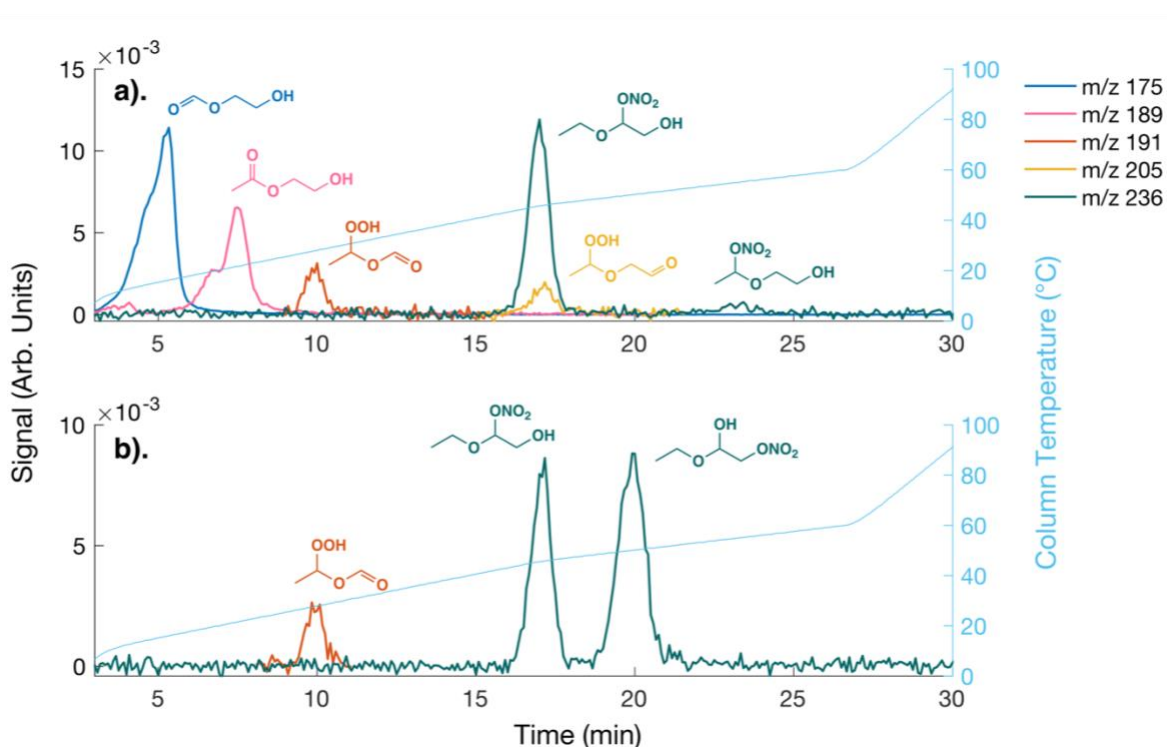

Figure S3. Gas chromatograms of oxidation products from NO experiments of **a).** 2-EE and **b).** EVE. Major products include: 2-OH-ethylformate (m/z 175), 3-R=O and 3-OH-R'CHO (m/z 189), 3-OOH-R'=O (m/z 191), 3-OOH-R'CHO (m/z 205), and the hydroxynitrates (m/z 236). The signal at m/z 175 is scaled down by a factor of 50, and the signal at m/z 189 is scaled down by a factor of 5.

In Figure S3(b), by comparing the gas chromatograms from 2-EE and EVE experiments, we assign the 1,2-hydroxynitrate (2-RONO$_2$) to the peak that elutes at lower temperature than the 2,1-hydroxynitrate peak. However, such assignment of the hydroxynitrates from EVE experiments is counterintuitive. Since the hydrogen-bonding interaction between the -OH group of 1,2-hydroxynitrate with the column should be stronger than that of the 2,1-hydroxynitrate due to less steric hindrance, we expect that 1,2-hydroxynitrate to elute later than the 2,1-hydroxynitrate. We speculate that the elution of 2,1-hydroxynitrate may be retarded by the

presence of the ether oxygen neighboring to the hydroxy group, which might strengthen the interaction between the -OH group and the column surface.

Another unusual phenomenon we observed in the NO experiments is the fast decay of CIMS signals of the hydroxynitrates (m/z 236). Shown in Figure S4 are the time series of m/z 236 from the NO experiments with 2-EE and EVE. We measure the overall loss rate for the nitrates from 2-EE experiment to be around 0.033 min^{-1}, and that from EVE experiment to be 0.037 min^{-1}. The loss of the nitrate signals is likely due to wall deposition, which may result from acid-catalyzed hydrolysis in the condensed phase.[24,25] We propose the possible hydrolysis mechanisms for the nitrates in Scheme S4.
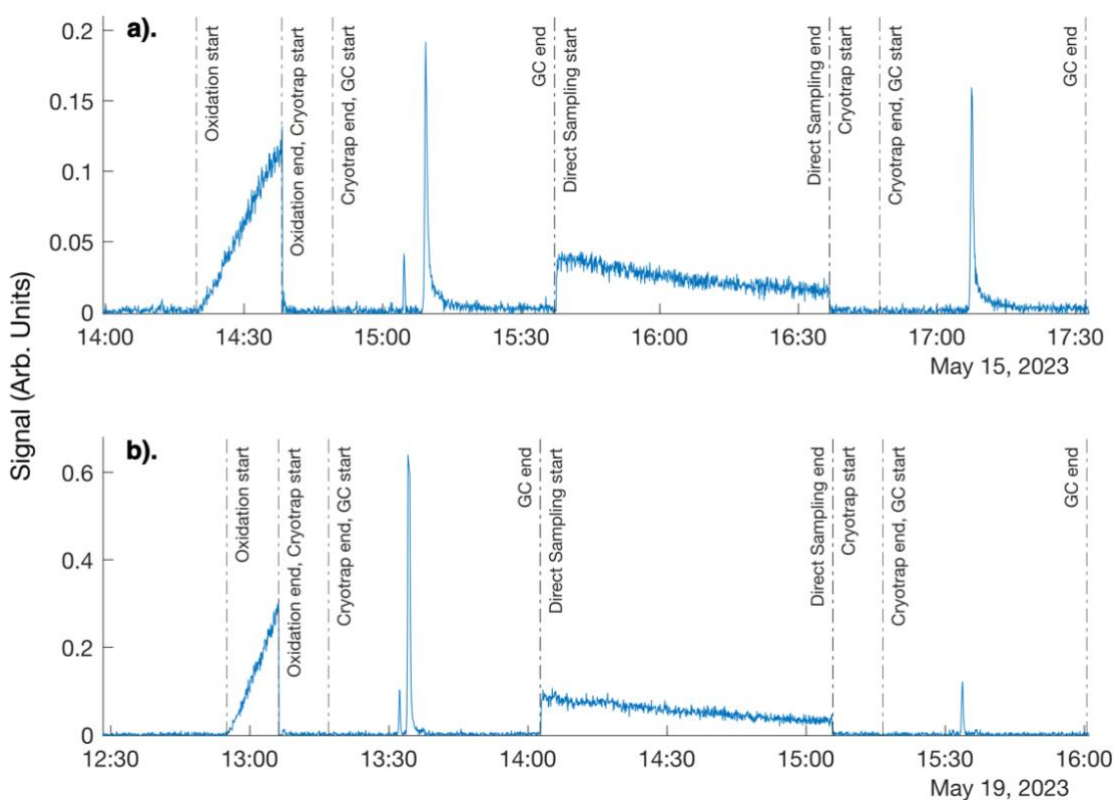

Figure S4. Time series of m/z 236 signals for **a).** a 2-EE experiment and **b).** an EVE experiment with NO. Important timesteps of GC-CIMS operation are denoted. The nitrate peaks are of different shapes and intensities from those in Figure S1 since the experiments are run under high sensitivity mode rather than normal mode (see Section S2), and fragmentation of the analytes at the ion source likely alters the GC signal.
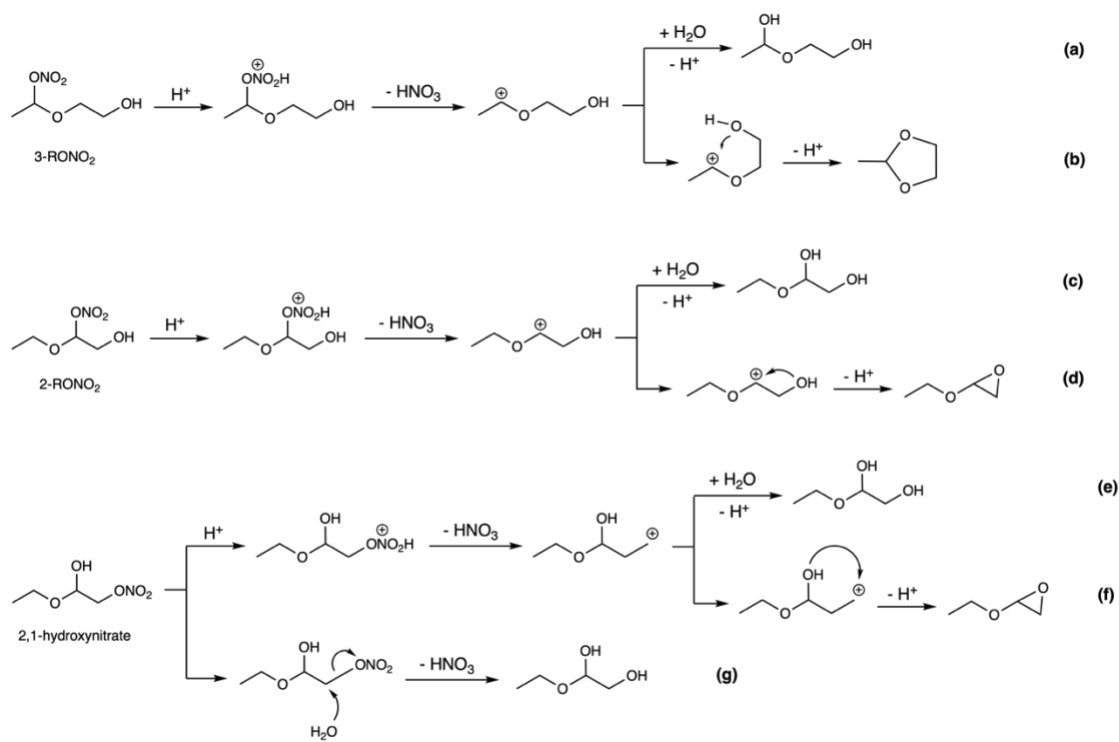
Scheme S4. Speculative hydrolysis mechanisms for hydroxynitrates observed in our experiments.

Shown in Figure S5 is the relationship between the concentrations of 3-R=O and 3-OH-R'CHO and the concentration of 2-OH-ethylformate from several 2-EE NO experiments. From the linear fitting, we determine that the yield of the two products from 3-RO isomerization relative to that of 2-OH-ethylformate is 0.095 ± 0.024.
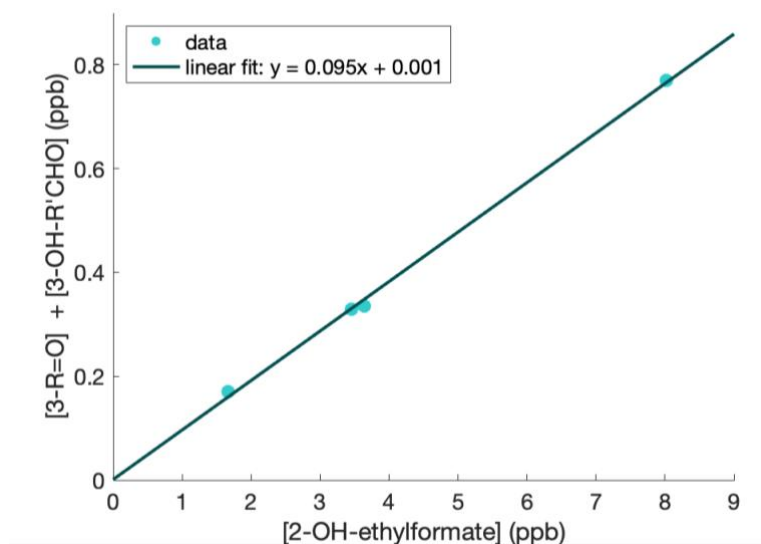

Figure S5. ([3-R=O] + [3-OH-R'CHO]) vs. [2-OH-ethylformate] from 2-EE NO experiments and the linear fit result.
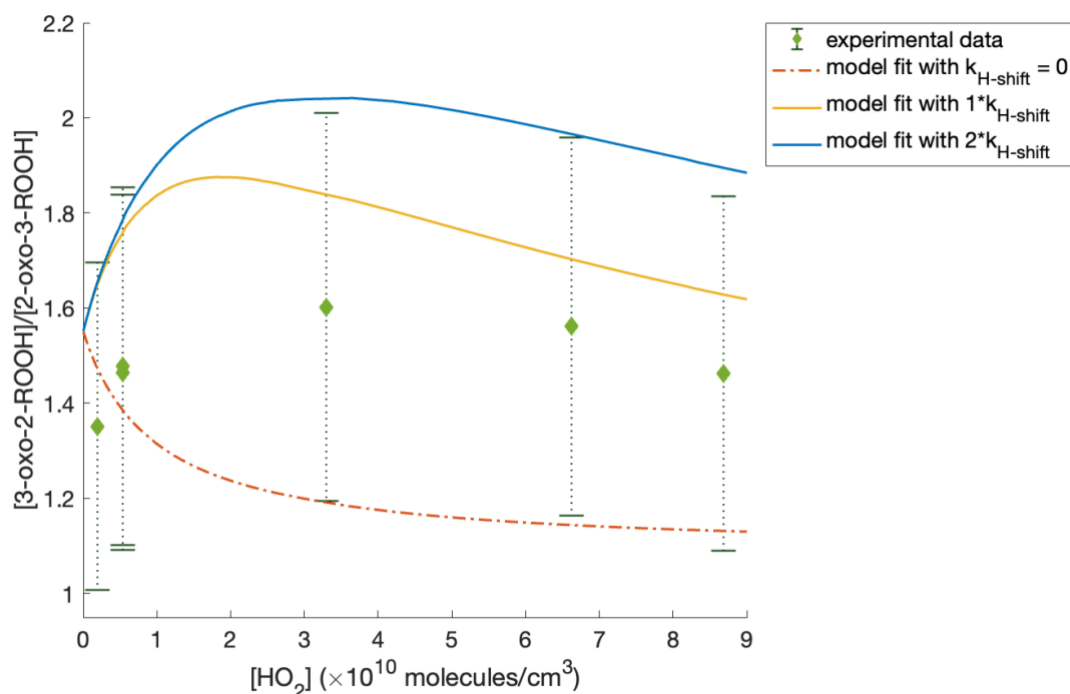
7.3 Additional Figures

Figure S6. [3-oxo-2-ROOH]/[2-oxo-3-ROOH] vs. [HO$_2$] at high temperature (309.5K). The data (in green markers) are from experiments at 309.5K. The orange dashed line is the result from model run without the 1,5 H-shift reaction of 2-OO-3-ROH radical, and the solid lines are results from model run with the 1,5 H-shift rate coefficient of 2-OO-3-ROH scaled by 1 and 2 times the calculated rate coefficients. The modelled outputs of the ratio between the two products seems to fail to fit well with the experimental results, and thus we refrain from providing an estimate for the 1,5 H-shift rate coefficient of 2-OO-3-ROH at high temperature. Still, at higher 1,5 H-shift rate, the modelled trend of the ratio obtains a similar shape with the trend from experimental results. The modelled results also fit within the error of experimental measurements, which mainly results from the uncertainties in the sensitivities of the compounds. Therefore, the seemingly divergence between the experimental and model results may be explained by the overestimation of the relative instrument sensitivities of 3-oxo-2-ROOH compared to 2-oxo-3-ROOH. The modelled trend of the ratio converges at ~1.55 at low [HO$_2$], which is slightly higher than that at room temperature (~1.43). The difference likely arises from the decrease in the rate coefficients of bimolecular reaction (RO$_2$+HO$_2$) at higher temperature.

References

(1)   Jenkin, M. E.; Valorso, R.; Aumont, B.; Rickard, A. R. Estimation of Rate Coefficients and Branching Ratios for Reactions of Organic Peroxy Radicals for Use in Automated Mechanism Construction. *Atmos. Chem. Phys.* **2019**, *19* (11), 7691–7717. https://doi.org/10.5194/ACP-19-7691-2019.

(2)   Praske, E.; Crounse, J. D.; Bates, K. H.; Kurtén, T.; Kjaergaard, H. G.; Wennberg, P. O. Atmospheric Fate of Methyl Vinyl Ketone: Peroxy Radical Reactions with NO and HO2. *J. Phys. Chem. A* **2015**, *119* (19), 4562–4572. https://doi.org/10.1021/jp5107058.

(3)   Calvert, J. G.; Mellouki, A.; Orlando, J. J.; Pilling, M. J.; Wallington, T. J. *The Mechanisms of Atmospheric Oxidation of the Oxygenates*; Oxford University Press, Inc., 2011.

(4)   Su, T.; Chesnavich, W. J. Parametrization of the Ion–Polar Molecule Collision Rate Constant by Trajectory Calculations. *J. Chem. Phys.* **1998**, *76* (10), 5183. https://doi.org/10.1063/1.442828.

(5)   Garden, A. L.; Paulot, F.; Crounse, J. D.; Maxwell-Cameron, I. J.; Wennberg, P. O.; Kjaergaard, H. G. Calculation of Conformationally Weighted Dipole Moments Useful in Ion–Molecule Collision Rate Estimates. *Chem. Phys. Lett.* **2009**, *474* (1–3), 45–50. https://doi.org/10.1016/J.CPLETT.2009.04.038.

(6)   Murphy, S. E.; Crounse, J. D.; Møller, K. H.; Rezgui, S. P.; Hafeman, N. J.; Park, J.; Kjaergaard, H. G.; Stoltz, B. M.; Wennberg, P. O. Accretion Product Formation in the Self-Reaction of Ethene-Derived Hydroxy Peroxy Radicals. *Environ. Sci. Atmos.* **2023**. https://doi.org/10.1039/D3EA00020F.

(7)   Martinez, R. D.; Buitrago, A. A.; Howell, N. W.; Hearn, C. H.; Joens, J. A. The near U.V. Absorption Spectra of Several Aliphatic Aldehydes and Ketones at 300 K. *Atmos. Environ. Part A. Gen. Top.* **1992**, *26* (5), 785–792. https://doi.org/10.1016/0960-1686(92)90238-G.

(8)   Messaadia, L.; El Dib, G.; Ferhati, A.; Roth, E.; Chakir, A. Gas Phase UV Absorption Cross-Sections for a Series of Hydroxycarbonyls. *Chem. Phys. Lett.* **2012**, *529*, 16–22. https://doi.org/10.1016/J.CPLETT.2012.01.044.

(9)   Bouzidi, H.; Aslan, L.; El Dib, G.; Coddeville, P.; Fittschen, C.; Tomas, A. Investigation of the Gas-Phase Photolysis and Temperature-Dependent OH Reaction Kinetics of 4-Hydroxy-2-Butanone. *Environ. Sci. Technol.* **2015**, *49* (20), 12178–12186. https://doi.org/10.1021/acs.est.5b02721.

(10)   Tadić, J.; Juranić, I.; Moortgat, G. K. Pressure Dependence of the Photooxidation of Selected Carbonyl Compounds in Air: N-Butanal and n-Pentanal. *J. Photochem. Photobiol. A Chem.* **2001**, *143* (2–3), 169–179. https://doi.org/10.1016/S1010-

6030(01)00524-X.

(11)   Yeh, G. K.; Ziemann, P. J. Gas-Wall Partitioning of Oxygenated Organic Compounds: Measurements, Structure-Activity Relationships, and Correlation with Gas Chromatographic Retention Factor. *Aerosol Sci. Technol.* **2015**, *49* (9), 727–738. https://doi.org/10.1080/02786826.2015.1068427.

(12)   Huang, Y.; Zhao, R.; Charan, S. M.; Kenseth, C. M.; Zhang, X.; Seinfeld, J. H. Unified Theory of Vapor-Wall Mass Transport in Teflon-Walled Environmental Chambers. *Environ. Sci. Technol.* **2018**, *52* (4), 2134–2142. https://doi.org/10.1021/acs.est.7b05575.

(13)   Zhang, X.; Schwantes, R. H.; McVay, R. C.; Lignell, H.; Coggon, M. M.; Flagan, R. C.; Seinfeld, J. H. Vapor Wall Deposition in Teflon Chambers. *Atmos. Chem. Phys.* **2015**, *15* (8), 4197–4214. https://doi.org/10.5194/ACP-15-4197-2015.

(14)   Brune, W. H. The Chamber Wall Index for Gas-Wall Interactions in Atmospheric Environmental Enclosures. *Environ. Sci. Technol.* **2019**, *53* (7), 3645–3652. https://doi.org/10.1021/acs.est.8b06260.

(15)   Compernolle, S.; Ceulemans, K.; Müller, J. F. Evaporation: A New Vapour Pressure Estimation Methodfor Organic Molecules Including Non-Additivity and Intramolecular Interactions. *Atmos. Chem. Phys.* **2011**, *11* (18), 9431–9450. https://doi.org/10.5194/ACP-11-9431-2011.

(16)   Vakhtin, A. B.; McCabe, D. C.; Ravishankara, A. R.; Leone, S. R. Low-Temperature Kinetics of the Reaction of the OH Radical with Hydrogen Peroxide†. *J. Phys. Chem. A* **2003**, *107* (49), 10642–10647. https://doi.org/10.1021/JP030424Q.

(17)   Hartmann, D.; Gedra, A.; Rhäsa, D.; Zellner, R. Rate Constants for Reaction of OH Radicals with Acetates and Glycols in the Gas Phase. *Physico-Chemical Behav. Atmos. Pollut.* **1987**, 225–235. https://doi.org/10.1007/978-94-009-3841-0_25.

(18)   Dagaut, P.; Liu, R.; Wallington, T. J.; Kurylo, M. J. Kinetic Measurements of the Gas-Phase Reactions of OH Radicals with Hydroxy Ethers, Hydroxy Ketones, and Keto Ethers. *J. Phys. Chem.* **1989**, *93* (23), 7838–7840. https://doi.org/10.1021/j100360a022.

(19)   Colmenar, I.; Salgado, S.; Martín, P.; Aranda, I.; Tapia, A.; Cabañas, B. Tropospheric Reactivity of 2-Ethoxyethanol with OH and NO3 Radicals and Cl Atoms. Kinetic and Mechanistic Study. *Atmos. Environ.* **2020**, *224*, 117367. https://doi.org/10.1016/j.atmosenv.2020.117367.

(20)   Stemmler, K.; Mengon, W.; Kerr, J. A. OH Radical Initiated Photooxidation of 2-Ethoxyethanol under Laboratory Conditions Related to the Troposphere: Product Studies and Proposed Mechanism. *Environ. Sci. Technol.* **1996**, *30* (11), 3385–3391. https://doi.org/10.1021/es960348n.

(21)   Burkholder, J. B.; Sander, S. P.; Abbatt, J. P. D.; Barker, J. R.; Huie, R. E.; Kolb, C. E.; Kurylo, M. J.; Orkin, V. L.; Wilmouth, D. M.; Wine, P. H. Chemical Kinetics and Photochemical Data for Use in Atmospheric Studies, Evaluation No. 19. *JPL Publ. 19-5* **2020**, No. 19, 1–153.

(22)   Stemmler, K.; Kinnison, D. J.; Alistair Kerr, J. Room Temperature Rate Coefficients for the Reactions of Oh Radicals with Some Monoethylene Glycol Monoalkyl Ethers. *J. Phys. Chem.* **1996**, *100* (6), 2114–2116. https://doi.org/10.1021/jp9520355.

(23)   Aschmann, S. M.; Atkinson, R. Kinetics of the Gas-Phase Reactions of the OH Radical with Selected Glycol Ethers, Glycols, and Alcohols. *Int. J. Chem. Kinet.* **1998**, *30* (8), 533–540. https://doi.org/10.1002/(SICI)1097-4601(1998)30:8<533::AID-KIN2>3.0.CO;2-T.

(24)   Liu, S.; Shilling, J. E.; Song, C.; Hiranuma, N.; Zaveri, R. A.; Russell, L. M. Hydrolysis of Organonitrate Functional Groups in Aerosol Particles. *Aerosol Sci. Technol.* **2012**, *46* (12), 1359–1369. https://doi.org/10.1080/02786826.2012.716175.

(25)   Wang, Y.; Piletic, I. R.; Takeuchi, M.; Xu, T.; France, S.; Ng, N. L. Synthesis and Hydrolysis of Atmospherically Relevant Monoterpene-Derived Organic Nitrates. *Environ. Sci. Technol.* **2021**, *55* (21), 14595–14606. https://doi.org/10.1021/acs.est.1c05310.